



Chemistry A European Journal

 **Chemistry
Europe**
European Chemical
Societies Publishing

Accepted Article

Title: Green, red and infrared emitting polymorphs of sterically hindered push-pull substituted stilbenes

Authors: Karel Pauk, Stanislav Luňák Jr., Aleš Růžička, Aneta Marková, Anna Mausová, Matouš Kratochvíl, Klára Melánová, Martin Weiter, Aleš Imramovský, and Martin Vala

This manuscript has been accepted after peer review and appears as an Accepted Article online prior to editing, proofing, and formal publication of the final Version of Record (VoR). This work is currently citable by using the Digital Object Identifier (DOI) given below. The VoR will be published online in Early View as soon as possible and may be different to this Accepted Article as a result of editing. Readers should obtain the VoR from the journal website shown below when it is published to ensure accuracy of information. The authors are responsible for the content of this Accepted Article.

To be cited as: *Chem. Eur. J.* 10.1002/chem.202004419

Link to VoR: <https://doi.org/10.1002/chem.202004419>

WILEY-VCH

FULL PAPER

Green, red and infrared emitting polymorphs of sterically hindered push-pull substituted stilbenes

Karel Pauk,^[b] Stanislav Luňák Jr.,^[a] Aleš Růžička,^[c] Aneta Marková,^[a] Anna Mausová,^[b] Matouš Kratochvíl,^[a] Klára Melánová,^[d] Martin Weiter,^[a] Aleš Imramovský,^[b] Martin Vala*^[a]

[a] Dr. S. Luňák Jr., MSc. A. Marková, MSc. M. Kratochvíl, Prof. M. Weiter, Assoc. Prof. M. Vala
Materials Research Centre, Faculty of Chemistry
Brno University of Technology
Purkyňova 464/118, CZ-612 00 Brno, Czech Republic
E-mail: vala@fch.vut.cz

[b] Dr. K. Pauk, Ms A. Mausová, Assoc. Prof. A. Imramovský
Institute of Organic Chemistry and Technology, Faculty of Chemical Technology
University of Pardubice
Studentská 95, CZ-530 09 Pardubice, Czech Republic

[c] Prof. A. Růžička
Department of General and Inorganic Chemistry, Faculty of Chemical Technology
University of Pardubice
Studentská 573, CZ-532 10 Pardubice, Czech Republic

[d] Dr. K. Melánová
Joint Laboratory of Solid State Chemistry, Faculty of Chemical Technology
University of Pardubice
Studentská 84, CZ-532 10 Pardubice, Czech Republic

Supporting information (full experimental and computational details for synthesis and analytics, single crystal XRD, powder XRD, spectral and photophysical measurements and quantum chemical calculations) for this article is given via a link at the end of the document.

Abstract: The synthesis, XRD single crystal structure, powder XRD and solid-state fluorescence of two new DPA-DPS-EWG derivatives (DPA = diphenylamino, DPS = 2,5-diphenyl-stilbene, EWG = carbaldehyde or dicyanovinylene) is described. Absorption and fluorescence maxima in solvents of various polarity show bathochromic shift with respect to parent DPA-stilbene-EWGs. Electronic coupling in dimers and potential twist elasticity of monomers were studied by density functional theory. Both polymorphs of CHO derivative emit green fluorescence (527 and 550 nm) of moderate intensity (10 % and 5 %) in polycrystalline powder form. Moderate (5 %) red (672 nm) monomer-like emission was also observed for the first polymorph of DCV derivative, while more intense (32 %) infrared (733 nm) emission of the second polymorph was ascribed to the excimer fluorescence.

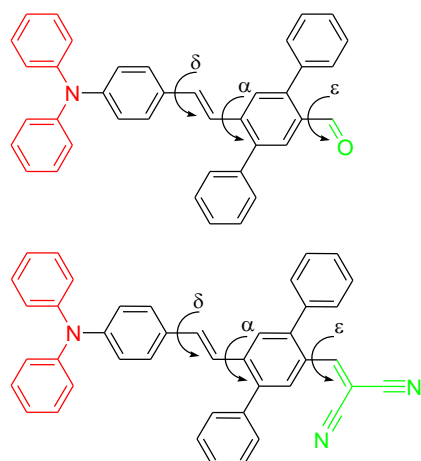
Introduction

Solid-state organic luminophors emitting in the far red / near infrared spectral region (FR / NIR, 650–900 nm [1] or 1000 nm [2]) are especially important in the fields of OLED and bioimaging [3]. Such low band-gap organic materials usually show lower photoluminescence quantum yields (PLQY) than emitters in shorter wavelength regions, because of intramolecular non radiative processes, preferred according to so-called „energy-gap“ law, and intermolecular formation of detrimental cofacial aggregates [2,4]. Common design of FR / NIR emitters consists of linking an electron donor and acceptor parts into one molecule in D- π -A [5], D- π -A- π -D [6] or A- π -D- π -A [7] fashion. D in these structures usually means diphenylamino or triphenylamino (DPA, TPA) type donor, while A is either heterocyclic acceptor [8], two or more cyano (CN) groups [9] or a combination of both [10]. In

2010 Shimizu and Hiyama expressed an essential requirement to obtain red fluorophores with PLQY over 30 % from neat solids and fulfilled it in 2012 by for first time observed emission with maximum over 700 nm (702 nm) and PLQY over 30 % (33 %) at the same time [11]. Although, since that time the impressive values of NIR emission were reported for polycrystalline powders, e.g. 735 nm / 11 % [9b], water dispersions of nanoparticles, e.g. 685 nm / 20.7 % [12], and neat films, e.g. 756 nm / 17 % [13] or 750 nm / 21 % [14], the >700 nm / >30 % limit still remains a challenge [15]. There are generally two ways to tune the position of emission maxima. The first one, intramolecular, modifies the strength of (usually) electron acceptor [14], e.g. by adding an additional CN group [10] or by a conjugation extension [16], while the second, intermolecular, modifies the structure in order to form emitting aggregates, e.g. of J-type [4c] or X-type [16]. Structural change, transforming the continuous H-type dimeric stacking to discrete dimers, showing intense (54.8 %) excimer fluorescence with a maximum at 690 nm, seems also promising [17].

Stilbene derivatives, substituted on central vinylene group by phenyls (tetraphenylethene, TPE), CN group (α -cyanostilbene, CS) or both (2,3,3-triphenylacrylonitrile, TPAN) form main substructures of the compounds showing aggregation-induced emission (AIE) or aggregation-induced enhanced emission (AIEE) [18]. If suitably substituted, their derivatives can show FR / NIR solid-state fluorescence (SSF) [19]. Earlier attempt to construct red emitting system of D- π -A type, using DPA donor and dicyanovinylene (DCV) complex acceptor, connected by 3D sterically hindered 9,9'-spirobifluorene, preventing the stacking, lead to intense SSF near 650 nm [20]. Thus, inspired by a stilbene versatility and DPA- π -DCV concept, we designed and synthesized **DPA-DPS-DCV**, with stilbene π -system substituted at acceptor part by a pair of phenyls (Scheme 1). 2,5-Diphenyl-stilbene (DPS) is thus a regioisomer of TPE. From another point

FULL PAPER

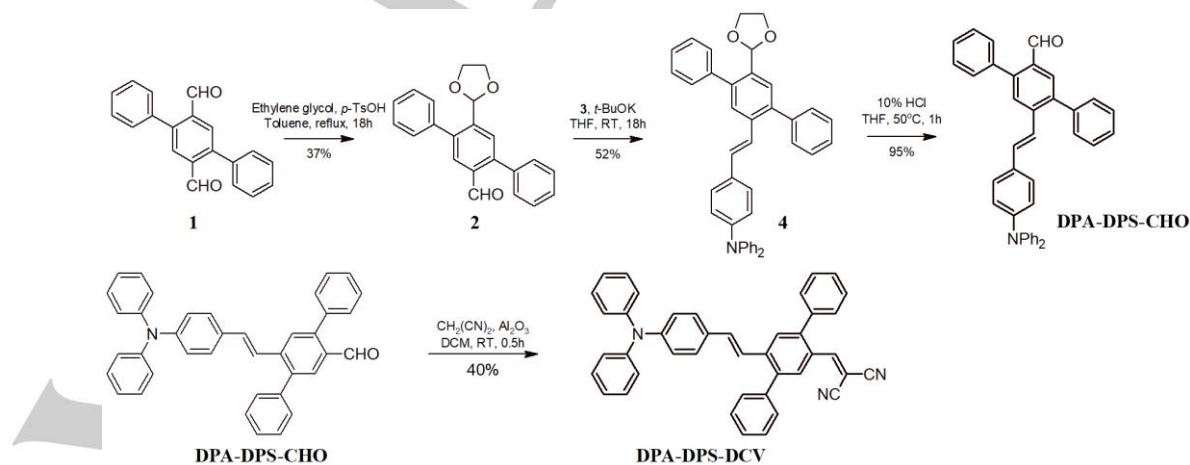


Scheme 1. Compounds under study, with highlighted D- π -A character by colour. Dihedral angles describe the rotation of a donor (δ) and acceptor (α) substituted parts of a stilbene core and the rotation of a substituent (ϵ).

of view, accenting the sterical hindrance between *ortho* phenyl and vinyl hydrogens, the compound can be considered as once by TPA and twice by CN substituted 2,5-diphenyl-1,4-divinylbenzene (PVB), i.e. TPA-PVB-(CN)₂. The polymorphism of propeller-like TPA containing fluorescent compounds is known [21] and is often used in stimuli-responsive materials [22]. Side phenyl substitution of *trans,trans*-distyrylbenzene lead to the formation of two polymorphs, showing either slipped-stacked or uncommon cross-stacked (X-type) packing [23]. As both these structural features are contained in the molecules under study, polymorphism is quite expectable.

Results and Discussion

The synthesis of the target compound was carried out according to Scheme 2. Although both final **DPA-DPS-DCV** and the key intermediate **DPA-DPS-CHO** have shown acceptable analytics (batch 1), the residual short wavelength fluorescence of an impurity in acetonitrile, where the infrared fluorescence of **DPA-DPS-DCV** is almost completely quenched, was observed.



Scheme 2. Synthesis of **DPA-DPS-CHO** and **DPA-DPS-DCV**. Compound 3, used in the second reaction step, is dimethyl [4-(diphenylamino)benzyl]phosphonate (see SI).

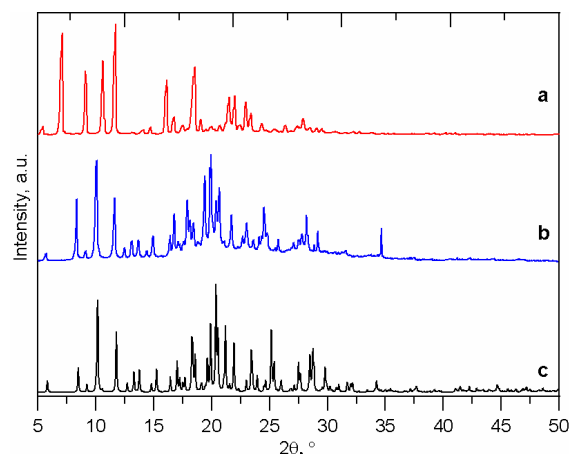


Figure 1. Normalized experimental PXRD of a) polymorph **R**, b) polymorph **IR** and c) recomputed from single crystal XRD of polymorph **IR**.

Thus, the synthesis was completely repeated and further purifying step (column chromatography) was included both, for **DPA-DPS-DCV** and for **-CHO**, before final crystallizations (batch 2). We were pleasantly surprised, that 1) the impurity emission disappeared, 2) **DPA-DPS-DCV** crystallized in a new modification with more intense SSF shifted to NIR and 3) the single crystal with sufficient parameters for X-ray diffractometry (XRD) was obtained. The crystal structure was also determined for **DPA-DPS-CHO** polymorph from batch 1. The existence of **DPA-DPS-DCV** polymorphs, coming from batch 1 (polymorph **R**) and batch 2 (polymorph **IR**) was confirmed by room temperature powder XRD (PXRD). The PXRD pattern, computed from low temperature single crystal XRD, agrees well with the experimental one for polymorph **IR** at lower θ (Fig. 1), while at the higher ones the differences caused by different temperature are more remarkable. The existence of two polymorphs of **DPA-DPS-CHO**, coming from batch 1 (polymorph **DG**) and batch 2 (polymorph **G**), was also confirmed by PXRD (Fig. S1).

FULL PAPER

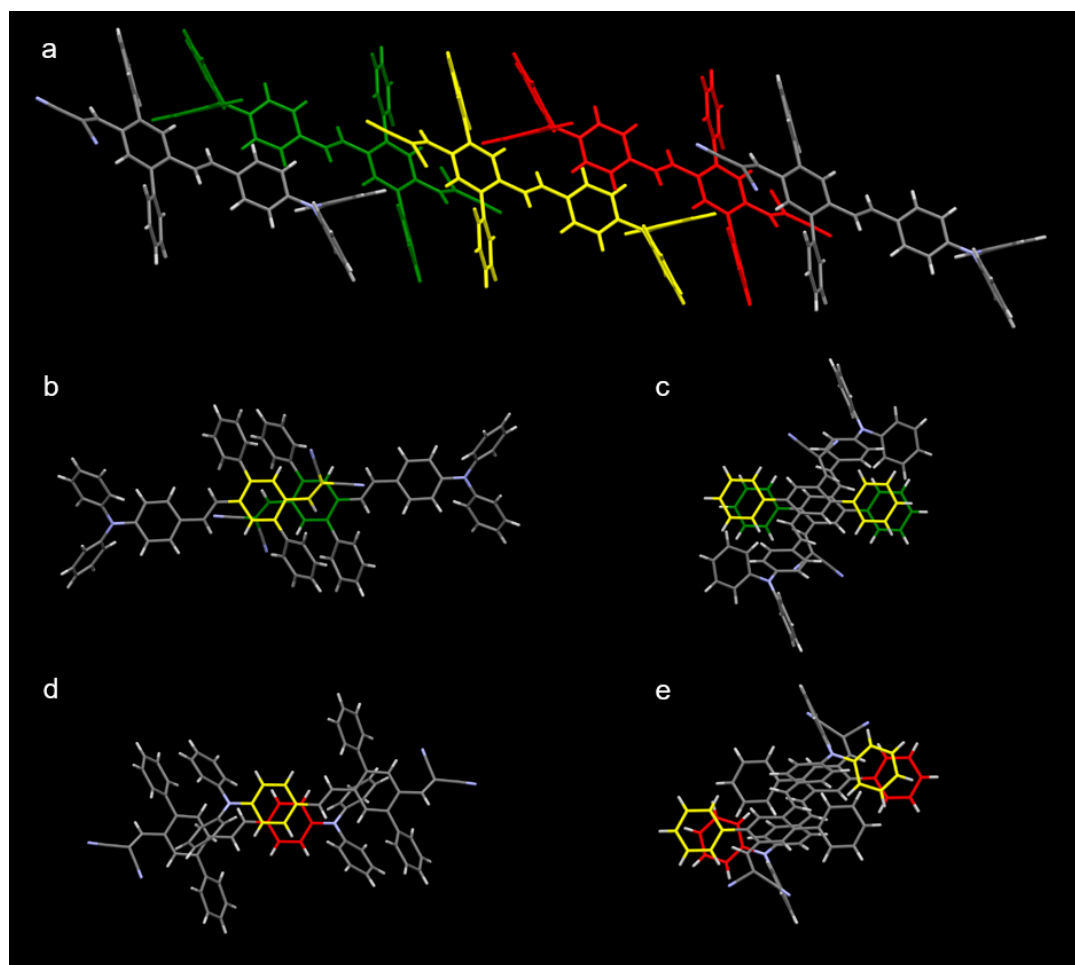


Figure 2. Crystal structure of polymorph IR. Overall view (a) on the alternation of the dimers in a slipped stacked column. Dimer 1 consists from yellow and green monomers, dimer 2 from yellow and red. Detail of dimer 1 (b, c) with highlighted stack (b) in a main conjugated chain ($\varphi = 32.9^\circ$, CC = 3.539 Å) and (c) between a pair of side phenyls ($\varphi = 13.1^\circ$, CC = 4.237 Å). Detail of dimer 2 (d, e) with highlighted stack (d) in a main conjugated chain ($\varphi = 0^\circ$, CC = 4.255 Å) and (e) between a side phenyl and phenyl from DPA group ($\varphi = 14.2^\circ$, CC = 4.054 Å).

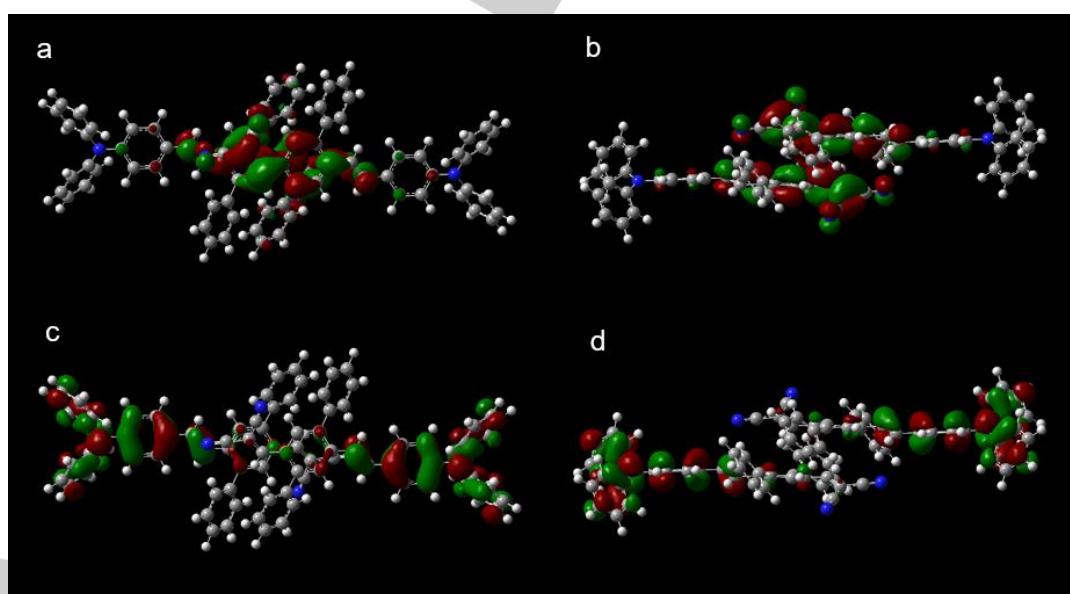


Figure 3. Splitting orbitals in dimer 1: LUMO+1 (a_g) (a, b), HOMO (a_u) (c, d), front view (a, c), side view (b, d), Isovalue = 0.02 was used for drawing.

FULL PAPER

DPA-DPS-CHO polymorph **DG** crystalizes in non-centrosymmetrical $P2_12_12_1$ space group, while **DPA-DPS-DCV** polymorph **IR** in centrosymmetrical $P1$ group. Consequently, in polymorph **DG** the charge separation, given by its push-pull character, is not compensated and the polymorph should show an activity in the second order nonlinear optics. On the other hand, the key structural feature of polymorph **IR** is the formation of highly slipped columns with two alternating types of centrosymmetrical dimers (Fig. 2a). The dominant type of packing is a formation of parallel offset face-to-face stacks [24], either between main conjugated chains or between side phenyls. The stacks were characterized by the angles φ between the planes of benzene rings (Fig. 2c-2e) or benzene ring and DCV group (Fig. 2b) and center-to-center (CC) distances (Fig. 2b-2e) and compared to density functional theory computed (DFT: ω B97X-D / 6-31G(d,p) [25]) optimized structure of benzene dimer ($\varphi = 0^\circ$, CC = 4.233 Å, Fig. S2a). Simply said, dimer 1 is more closely π -stacked along the main conjugated chain with plane-to-plane (PP, defined by the central rings of PVB substructure) distance 3.378 Å (Fig. S3a), while the dimer 2 is more loosely stacked with PP, defined by TPA phenyls, equal to 3.952 Å (Fig. S3b), but a bit better stacked between side phenyl and DPA phenyl (Fig. 2e), than dimer 1 between side phenyls of PVB (Fig. 2c).

Geometry of both alternating dimers 1 and 2 was recomputed from crystal structures by density functional theory (DFT) and compared with the experimental data (Fig. S3), in order to understand 1) how stand-alone are both dimers in an isolated dimer approximation, and 2) how their arrangement affects the electronic structure (Fig. 3). Computed structure of dimer 1 matches the experiment in an excellent way. The crucial stack between benzene ring and vinylene of DCV gives CC = 3.485 Å (exp. CC = 3.539 Å), an overall length of a conjugated system of a dimer, characterized by a distance between the nitrogens of TPA groups (NN), is 22.508 Å (exp. NN = 22.536 Å). The plane-to-plane (PP) distance between planes, defined by central benzene rings of PVB, is 3.238 Å (exp. PP = 3.378 Å), indicating a bit overestimated attractive forces in DFT calculations. Consequently, the computed PP = 3.395 Å and CC = 3.795 Å in a benzene parallel offset stack (Fig. S2a) may be also lower than the real ones and thus the experimental values of CCs between side phenyls (Fig. 2c, e) may be relatively close to the ideal phenyl-phenyl stack. On the other hand, there is a considerable difference between the computed and experimental parameters of dimer 2: PP = 3.660 Å (exp. PP = 3.952 Å) and NN = 8.210 Å (exp. NN = 7.824 Å), i.e. the computed geometry is compressed in a perpendicular direction and prolonged along the direction of a conjugated system (Fig. S3b). The dimer 1 thus can be considered as a discrete dimer [26], while the dimer 2 is not stand-alone, as its structure significantly depends on interactions with further neighbours, omitted in a dimer approximation.

Both frontier Kohn-Sham orbitals of a monomer are splitted in a dimer. These splitted orbitals in a centrosymmetrical dimer are of a_g and a_u symmetry. Their shape thus differs mainly by the opposite parity and their energy difference relates to electronic coupling, i.e. hole and electron transfer integrals [27]. These splittings are relatively small in dimer 2 (Δ HOMO = 22 meV, Δ LUMO = 51 meV), for dimer 1 Δ HOMO = 45 meV remains also small, while Δ LUMO = 234 meV is considerably higher. The size of orbital energy splittings is reflected in a shape of these MOs (Figs. 3, S4). HOMO orbitals on monomers do not overlap in any

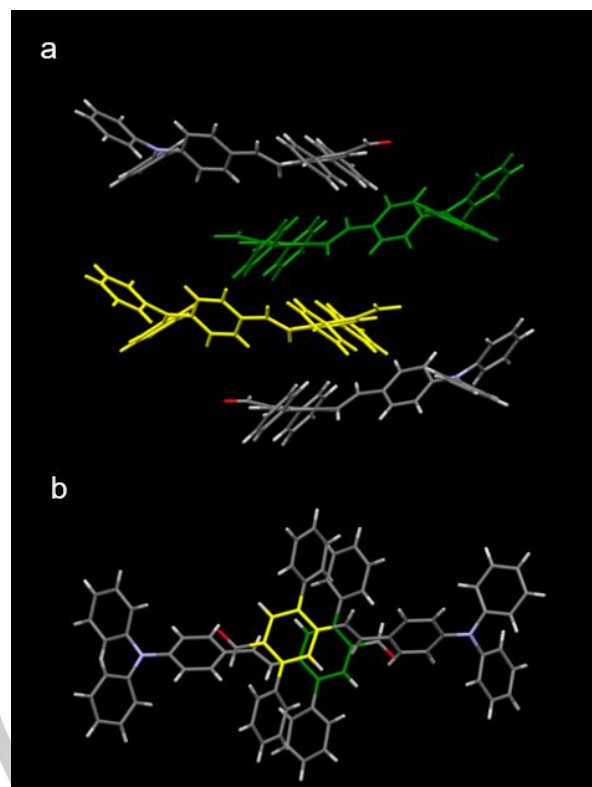


Figure 4. Crystal structure of polymorph **DG**. Overall view (a) on the stacked column. Detail of a dimer (b) with highlighted stack in a main conjugated chain ($\varphi = 12.3^\circ$, CC = 4.888 Å).

dimer, so as any of splitted LUMO orbitals for dimer 2, but the LUMOs in dimer 1 share a common space at the vinylene-benzene part, as seen from the side view on Fig. 3. After the excitation to LUMO electron can easily move between both monomers of dimer 1, but not out of them, while hole must stay located on one of TPA groups. Such situation is ideal for a formation of an excimer, localized on dimer 1.

The packing of **DPA-DPS-CHO** in polymorph **DG** is considerably different. Molecules form infinite columns, consisting of the same type of non-centrosymmetrical dimers (Fig. 4). The key intermolecular interaction is an edge-to-face γ -shaped [24] arrangement of the side phenyls (Fig. S5), in which all these phenyls serve both as donors and acceptors in C-H \cdots π interactions. The effective stack between main conjugated chains of adjacent molecules in a column is disabled, because of big CC distance (Fig. 4). Consequently, there is no efficient electronic coupling between conjugated chains, and the molecules can be considered as electronically isolated monomers. If the parameters of side phenyl edge-to-face arrangement (Fig. S5) are compared with DFT optimized structure of corresponding benzene dimer ($\varphi = 75.9^\circ$, CC = 4.841 Å, Fig. S2b), we see that the values from crystal are quite close to the ideal phenyl-phenyl γ -shaped arrangement.

Molecular geometries of both **DPA-DPS-DCV** and **DPA-DPS-CHO** in crystals are quite similar (Fig. 5). Both crystals contain only one independent molecule, side phenyls are nearly coplanar, rotated about 50° out-of-plane for both molecules and show *anti* arrangement on acceptor substituted part of stilbene, characterized (Scheme 1) by dihedral angles $\alpha = 40.1^\circ$ and

FULL PAPER

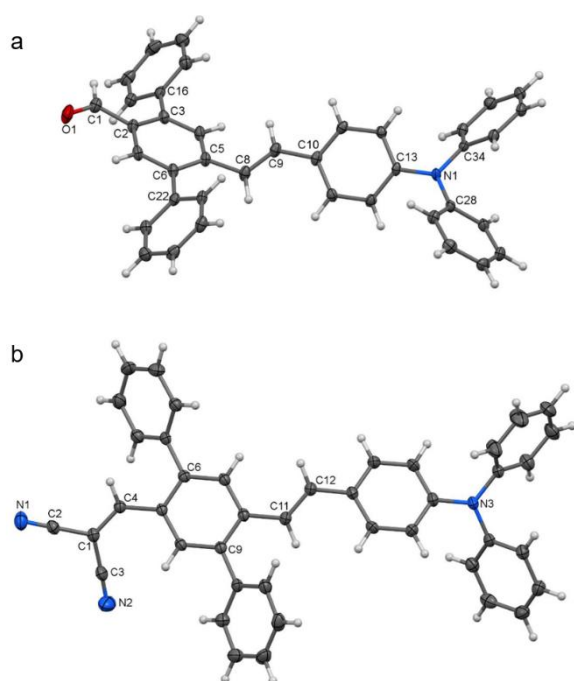


Figure 5. Molecular structure of **DPA-DPS-CHO** (a) and **DPA-DPS-DCV** (b), ORTEP view, 50% probability level.

$\varepsilon = -10.6^\circ$ (CHO) and $\alpha = -16.5^\circ$ and $\varepsilon = 31.1^\circ$ (DCV). On the contrary electron donating TPA groups are rotated in an opposite sense with respect to α , giving $\delta = 7.0^\circ$ (CHO) and $\delta = 21.8^\circ$ (DCV), but the sum of absolute values of $\alpha + \delta$ does not differ considerably for both compounds. On the other hand, crystal of DPA-stilbene-CHO [28] contains two independent molecules, one of them in *anti* ($\alpha = 8.9^\circ$ and $\varepsilon = -0.6^\circ$, $\delta = 3.4^\circ$) and the second in *syn* ($\alpha = -1.9^\circ$ and $\varepsilon = 168.6^\circ$, $\delta = 11.2^\circ$) arrangement. Molecular modelling (Tab. S2) shows marginal energy differences between rotamers with *syn* and *anti* arrangements for DPA-stilbene-EWG derivatives (<0.012 kcal/mol) and more than the order of magnitude higher for DPA-DPS-EWG derivatives (>3.055 kcal/mol). Thus the steric hindrance of side phenyl substituents causes two structural effects: more pronounced non-planarity of a main conjugated chain and fixation a *anti* conformer. The potential minimum, relating to the conformer with an opposite sense of TPA rotation, was found only for both CHO derivatives and the energy difference between both rotamers of **DPA-DPS-CHO** was marginal (<0.2 kcal/mol). Thus the conformation of **DPA-DPS-DCV** molecule, observed in crystal, is the only one preferred by theory, while the experimental conformation of **DPA-DPS-CHO** is one of at least two favourable rotamers. The ability to undergo substantial changes of a dihedral angle between donor and acceptor parts of a molecule, depending on the external stimuli, can be considered as „twist elasticity“ and may be a source of polymorphism of **DPA-DPS-CHO** [29].

Absorption and fluorescence were studied in five solvents of various polarity (Fig. 6, Tab. S1). **DPA-DPS-CHO** behaves in solution in a similar way as other compounds of DPA- π -CHO

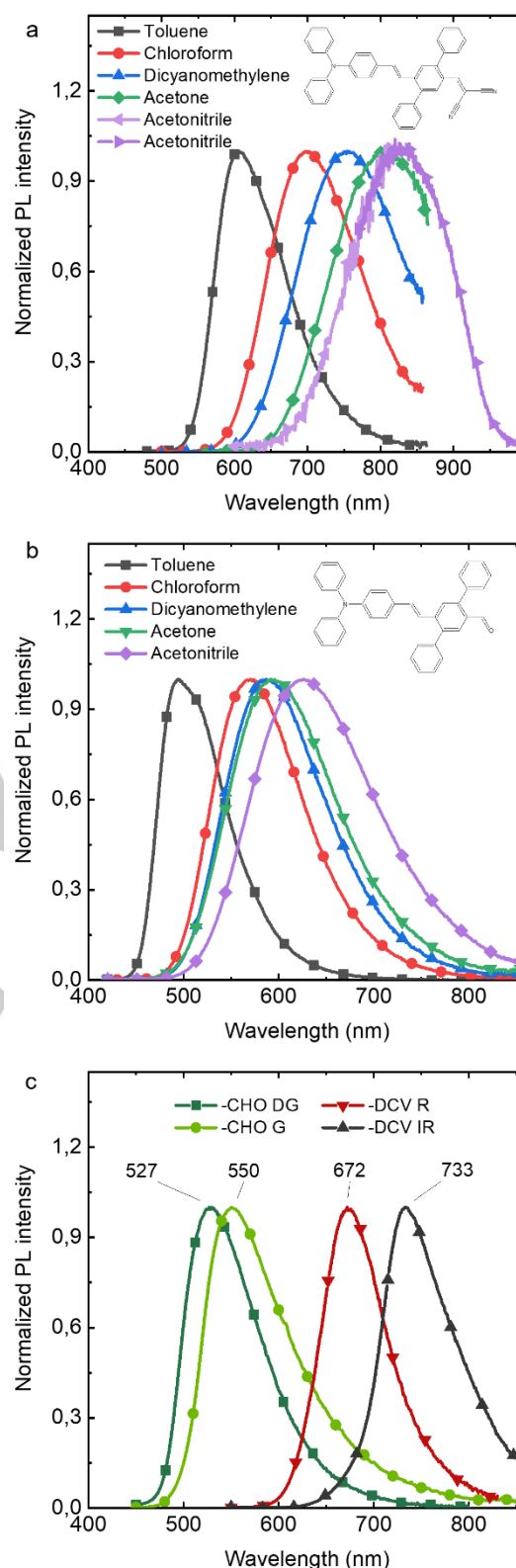


Figure 6. Fluorescence spectra of **DPA-DPS-CHO** (a) and **DPA-DPS-DCV** (b) in various solvents, and all polymorphs in powder (c). Maximum of very weak fluorescence of **DPA-DPS-DCV** in acetonitrile was near the end of a detection range of a conventional spectrofluorometer, so it was extended with the laser excited NIR emission detected with iCCD camera.

FULL PAPER

structure [30]. The absorption maximum in toluene is 3 nm red shifted with respect to DPA-stilbene-CHO [30a], molar absorptivity is lower, as side phenyls do not contribute to the oscillator strength and only increase a molecular weight, fluorescence maximum is 13 nm red shifted and PLQY and fluorescence lifetime (τ_F) are almost identical. The dependence of the absorption and fluorescence on solvent polarity is quite similar to DPA-biphenyl-CHO [30b], i.e. the absorption maxima are not significantly affected by solvents, while the fluorescence shows a remarkable red shift with increasing polarity, that is a common feature of D- π -A molecules, arising from intramolecular charge-transfer [9a]. The highest PLQY is reached for solvents with medium polarity as for DPA-biphenyl-CHO [30b], but its decrease in high polarity solvents is not so dramatic. On the other hand, the differences between spectral and photophysical properties of **DPA-DPS-DCV** and DPA-stilbene-DCV [31] are remarkable (Tab. S1). First of all, the absorption maxima of **DPA-DPS-DCV** in the same (dichloromethane) or similar (benzene and toluene) solvents are dramatically red shifted (from 395 to 473 nm and from 394 to 470 nm, respectively). Even bigger shifts are observed for fluorescence maxima (from 524 to 752 nm in dichloromethane and from 488 nm in benzene to 605 nm in toluene). PLQYs of **DPA-DPS-DCV** are higher in less polar solvents and lower in the more polar ones, as compared to DPA-stilbene-DCV. Furthermore, theoretical calculation, based on time dependent (TD) DFT / DFT (Tab. S2), predict exactly the opposite effect, i.e. a hypsochromic shift in absorption, caused by the decreased planarity of a conjugated chain between electron donor and acceptor, due to side-phenyl hindrance. Strictly said, we are unable to explain the slight (CHO) or dramatic (DCV) bathochromic shifts, induced by side-phenyl substitutions. We may only speculate, that the correct description of both absorbing and emitting states of these push-pull stilbenes in solution requires an involvement of charge-transfer structures, as in merocyanines [31], contributing a bit (CHO) or considerably more (DCV) in screwed side-phenyl substituted derivatives, as compared to DPA-stilbene-EWGs.

SSF of polycrystalline powders of both polymorphs of both compounds is shown on Fig. 6c. **DPA-DPS-CHO** polymorphs emit green fluorescence with the maxima at 527 nm (**DG**) and 550 nm (**G**) and with moderate PLQY 10 % (**DG**) and 5 % (**G**). Polymorph **DG** with known XRD structure emits without doubts as an isolated monomer, because of a marginal electronic coupling between its molecules. As the packing in polymorph **G** is not known, we may only speculate, that, due to the twist elasticity, the bathofluoric shift and the decrease of PLQY may come from the arrangement with less distorted monomer conformation and with tighter packing as for bis-TPA substituted thiazolothiazol [21b]. PLQY of both polymorphs is lower than for any solvent, so neither TPA group, as expected [18a], nor DPS bridge, on the contrary to TPE regioisomer [18a], can be considered as AIEgens. **DPA-DPS-DCV** polymorphs emit in target FR / NIR area with moderate intensity for polymorph **R** (672 nm, 5 %) and more intensely for polymorph **IR** (733 nm, 32 %), i.e. with parameters only rarely reported, e.g. for four-coordinated boron compounds [33]. We consider the red emission as coming from an isolated monomer in analogy with both green emitters, while the NIR emission as coming from excimer fluorescence located on dimer 1 (Fig. 2b). As compared to fluorescence in solvents, the emissions of electronically isolated monomers with 5 % PLQY (**G** and **R**) thus lie at the wavelengths 20–30 nm shorter than in chloroform, due

to their limited ability of excited state relaxation, as compared to fluid environment. Further support of this interpretation comes from apparent similarity of the crystal structure and spectral and photophysical behaviour of **R** and **IR** polymorphs with the recently reported excimer type emitter BTA-TPA [19b]. The structural similarity consists of the alternation of the stacked discrete dimer (PP = 3.38 Å for **IR** polymorph and 3.50 Å for BTA-TPA) with the unstacked one (PP = 3.95 Å for **IR** polymorph and 4.31 Å for BTA-TPA). Both compounds show a considerable blue-shift of SSF, if going from excimer type fluorescence to the monomer type (going from polymorph **IR** to **R** in our case, from crystal to amorphous film for BTA-TPA), accompanied by a decrease of PLQY (from 32 % for **IR** to 5 % for **R**, from 54.8 % for crystal to 21.9 % for amorphous film) and fluorescence lifetime (from 4.52 ns for **IR** to 1.46 ns for **R** [34], from 6.8 ns for crystal to 3.7 ns for amorphous film of BTA-TPA). Both, the polymorph **IR**, and BTA-TPA fluorescence lifetime of excimer fluorescence is remarkably longer than in any reported solvent, in which, in addition, the decay is always monoexponential (Tab. S1).

We note only, that the **IR** polymorph is sufficiently stable. There were found no significant changes in single crystal XRD after several months standing in a deposit. SSF of polycrystalline powder was also well reproduced. On the other hand, if the powder is pressed between two glasses, its fluorescence maximum shows immediate hypsochromic shift to about 670 nm, i.e. near to the maximum of polymorph **R**, so **IR** polymorph can be considered as stimuli-responsive.

Conclusion

Decorating of push-pull substituted stilbenes with a pair of side phenyls fixes and screws the molecular structure and causes bathochromic and bathofluoric spectral shift in solutions. Both compounds form polymorphs, which show solid-state fluorescence in a polycrystalline powder form. On the contrary to its TPE regioisomer, 2,5-diphenyl-stilbene π -bridge is not an AIEgen. Interactions of side phenyl pairs are decisive for a packing in crystals and consequently for spectral position and intensity of SSF. Their edge-to-face arrangement lead to minimal electronic coupling of molecular main conjugated chains and an emission of moderate intensity comes from relatively isolated monomers in crystals. Parallel offset face-to-face packing of side phenyls enabled to form crystal consisting of the electronically coupled isolated dimers, showing rare excimer type intense emission in near infrared region.

Experimental Section

Synthesis All reagents and solvents were purchased from commercial sources (Sigma-Aldrich, Fluorochem, Acros Organics, TCI Europe, Merck, and Lach-Ner). Commercial grade reagents were used without further purification. Tetrahydrofuran (THF) was pre-dried under sodium and then distilled under a nitrogen atmosphere. Reactions were monitored using thin layer chromatography (TLC) plates coated with 0.2 mm silica gel (60 F254, Merck). TLC plates were visualized using UV irradiation (254 nm). All melting points were determined using a Melting Point B-540 apparatus (Büchi, Switzerland) and are given in their uncorrected form. The IR spectra were recorded on a Nicolet 6700 FT-IR spectrometer (Thermo Fisher Scientific, Wal-tham, MA, USA) over the range of 400–4000 cm^{-1} using the ATR technique. The NMR spectra were measured in DMSO- d_6 ,

FULL PAPER

CDCl₃, CD₂Cl₂-d₂, and Tetrahydrofuran-d₈ (TDF) solutions at ambient temperature on a Bruker Avance™ III 400 spectrometer at frequencies 400 MHz (1H) and 100.26 MHz (13C), or on a Bruker Ascend™ 500 spectrometer at frequencies 500.13 MHz (1H) and 125.76 MHz (13C(1H)). The chemical shifts (δ) reported in SI are given in ppm and are related to the following residual solvent peaks: -4.79 (D₂O-d₂), -5.32 (CD₂Cl₂-d₂), -7.27 (CDCl₃), and -2.5 (DMSO-d₆). Tetramethylsilane (TMS) was used as an internal standard. The coupling constants (*J*) are reported in Hz. Elemental analyses (C, H, and N) were performed on an automatic microanalyser (Flash 2000 Organic elemental analyser). Mass spectrometry with high resolution was determined by the "dried droplet" method using a MALDI mass spectrometer LTQ Orbitrap XL (Thermo Fisher Scientific) equipped with a nitrogen UV laser (337 nm, 60 Hz). Spectra were measured in positive ion mode and in regular mass extent with a resolution of 100,000 at a mass-to-charge ratio (*m/z*) of 400, with 2,5-dihydrobenzoic acid (DBH) used as the matrix. The FT-IR spectra were recorded on FT-IR Nicolet iS50 using the ATR technique.

Single crystal XRD Full-sets of diffraction data were collected at 150(2)K with a Bruker D8-Venture diffractometer equipped with Cu (Cu/K_α radiation; λ = 1.54178 Å) or Mo (Mo/K_α radiation; λ = 0.71073 Å) microfocus X-ray (μs) sources, Photon CMOS detector and Oxford Cryosystems cooling device was used for data collection. The frames were integrated with the Bruker SAINT software package using a narrow-frame algorithm. Data were corrected for absorption effects using the Multi-Scan method (SADABS). Obtained data were treated by XT-version 2017/1 and SHELXL-2014/7 software implemented in APEX3 v2017.1-0 (Bruker AXS) system. Crystallographic data for structural analysis have been deposited with the Cambridge Crystallographic Data Centre, CCDC nos. 1964768-1964769.

Powder XRD Powder X-ray diffraction data were obtained with a D8 Advance diffractometer (Bruker AXS, Germany) with Bragg-Brentano θ-θ geometry (30 kV, 20 mA) equipped with Ni-β filter and a LynxEye detector using Cu K_α radiation. The scan was performed at room temperature from 2° to 70° (2θ) in 0.01° steps with a counting time of 2 s per step.

Spectral and photophysical measurements The UV-Vis absorption was measured employing Varian Cary Probe 50 UV-Vis spectrometer (Agilent Technologies Inc.). The steady state photoluminescence was captured using SF5 spectrofluorometer (Edinburgh Instruments). The photoluminescence quantum yields (PLQYs) were determined by absolute method employing integrating sphere SC-30 (Edinburgh Instruments). PLQYs of powdered samples were determined by combination of direct and indirect excitation. The fluorescence in the 800-1000 nm range was measured using Andor Shamrock spectrograph SR-303i-B equipped with iCCD istars DH740-18U-03 camera (Andor Technology). The sample was excited by laser pulses from EKSPLA PG400 Nd:YAG laser with H400 harmonic generator and PG 401 tuneable picosecond OPA. Time-resolved fluorescence was recorded by means of the time correlated single photon counting method (TCSPC) with a Horiba Jobin Yvon Fluorocube.

Quantum chemical calculations Geometry of monomers of both **DPA-DPS-DCV** and **-CHO** and centrosymmetrical dimers of **DPA-DPS-DCV**, extracted from experimental XRD, were recomputed by density functional theory (DFT) using ωB97X-D xc functionals and with 6-31G(d,p) basis set. The computed geometries of monomers were checked by vibrational analysis. All calculations were carried out with Gaussian 09 software. The resulting geometries of the dimers were characterized by plane-to-plane (PP) and centre-to-centre (CC) distances between the rings. Excitation energies were calculated by TD DFT ωB97X-D / 6-31+G(d,p) level. All calculations were carried out in vacuum.

Acknowledgements

This work was supported by the Czech Science Foundation grant No. 17-21105S. Access to computing and storage facilities owned by parties and projects contributing to the National Grid Infrastructure MetaCentrum provided under the programme "Projects of Large Research, Development, and Innovations Infrastructures" (CESNET LM2015042) is greatly appreciated by S.L.

Keywords: Donor-acceptor systems • Fluorescence • Density functional calculations • Crystal engineering • Polymorphism

- [1] J. Mei, Y. Huang, H. Tian, *ACS Appl. Mater. Interfaces* **2018**, *10*, 12217-12261.
- [2] A. Zampetti, A. Minotto, F. Cacialli, *Adv. Funct. Mater.* **2019**, *29*, 1807623.
- [3] Q. Zhao, J.Z. Sun, *J. Mater. Chem. C* **2016**, *4*, 10588-10609.
- [4] a) J.H. Kim, J.H. Yun, J.Y. Lee, *Adv. Opt. Mater.* **2018**, *6*, 1800255; b) Q. Wei, N. Fei, A. Islam, T. Lei, L. Hong, R. Peng, X. Fan, L. Chen, P. Gao, Z. Ge, *Adv. Opt. Mater.* **2018**, *6*, 1800512; c) J. Xue, Q. Liang, R. Wang, J. Hou, W. Li, Q. Peng, Z. Shuai, J. Qiao, *Adv. Mater.* **2019**, *31*, 1808242.
- [5] C. Li, R. Duan, B. Liang, G. Han, S. Wang, K. Ye, Y. Liu, Y. Yi, Y. Wang, *Angew. Chem. Int. Edit.* **2017**, *56*, 11525-211529.
- [6] S. Wang, X. Yan, Z. Cheng, H. Zhang, Y. Liu, Y. Wang, *Angew. Chem. Int. Edit.* **2014**, *53*, 2119-2123.
- [7] L. Yao, S. Zhang, R. Wang, W. Li, F. Shen, B. Yang, Y. Ma, *Angew. Chem. Int. Edit.* **2015**, *54*, 13068-13072.
- [8] T. Liu, L. Zhu, C. Zhong, G. Xie, S. Gong, J. Fang, D. Ma, C. Yang, *Adv. Funct. Mater.* **2017**, *27*, 1606384.
- [9] a) X. Han, Q. Bai, L. Yao, H. Liu, Y. Gao, J. Li, L. Liu, Y. Liu, X. Li, P. Lu, B. Yang, *Adv. Funct. Mater.* **2015**, *25*, 7521-7529; b) S. Redon, G. Eucat, M. Ipuay, E. Jeanneau, I. Gautier-Luneau, A. Ibanez, C. Andraud, Y. Bretonnière, *Dyes Pigm.* **2018**, *156*, 116-132.
- [10] D.G. Congrave, B.H. Drummond, P.J. Conaghan, H. Francis, S.T.E. Jones, C.P. Grey, N.C. Greenham, D. Credgington, H. Bronstein, *J. Am. Chem. Soc.* **2019**, *141*, 18390-18394.
- [11] M. Shimizu, T. Hiyama, *Chem. Asian J.* **2010**, *5*, 1516-1531; b) M. Shimizu, R. Kaki, Y. Takeda, T. Hiyama, N. Nagai, H. Yamagishi, H. Furutani, *Angew. Chem. Int. Edit.* **2012**, *51*, 4095-4099.
- [12] J. Qi, X. Duan, Y. Cai, S. Jia, C. Chen, Z. Zhao, Y. Li, H.Q. Peng, R.T.K. Kwok, J.W.Y. Lam, D. Ding, B.Z. Tang, *Chem. Sci.* **2020**, *11*, 8438-8477.
- [13] Y. Yuan, Y. Hu, Y.X. Zhang, J.D. Lin, Y.K. Wang, Z.Q. Jiang, L.S. Liao, S.T. Lee, *Adv. Funct. Mater.* **2017**, *27*, 1700986.
- [14] J. Kumsampao, C. Chaiwai, P. Chasing, T. Chawanpunyawat, S. Namuangruk, T. Sudyoasduk, V. Promarak, *Chem. Asian J.* **2020**, *15*, 10.1002/asia.202000727.
- [15] H. Lu, Y. Zheng, X. Zhao, L. Wang, S. Ma, X. Han, B. Xu, W. Tian, H. Gao, *Angew. Chem. Int. Edit.* **2016**, *55*, 155-159.
- [16] Y.J. Yu, Y. Hu, S.Y. Yang, W. Luo, Y. Yuan, C.C. Peng, J.F. Liu, A. Khan, Z.Q. Jiang, L.S. Liao, *Angew. Chem. Int. Edit.* **2020**, *10.1002/anie.202006197.*
- [17] a) Z. Sun, Q. Zang, Q. Luo, C. Lv, F. Cao, Q. Song, R. Zhao, Y. Zhang, W.Y. Wong, *Chem. Commun.* **2019**, *55*, 4735-4738; b) Q. Luo, L. Li, H. Ma, C. Lv, X. Jiang, X. Gu, Z. An, B. Zou, C. Zhang, Y. Zhang, *Chem. Sci.* **2020**, *11*, 6020-6025.
- [18] J. Mei, N.L.C. Leung, R.T.K. Kwok, J.W.Y. Lam, B.Z. Tang, *Chem. Rev.* **2015**, *115*, 11718-11940; b) M. Martínez-Abadía, R. Giménez, M.B. Ros, *Adv. Mater.* **2018**, *30*, 1704161.
- [19] M. Kang, X. Gu, R.T.K. Kwok, C.W.T. Leung, J.W.Y. Lam, F. Li, B.Z. Tang, *Chem. Commun.* **2016**, *52*, 5957-5960; b) Y. Zhang, J. Zhang, J. Shen, J. Sun, K. Wang, Z. Xie, H. Gao, B. Zou, *Adv. Opt. Mater.* **2018**, *6*, 18009565.
- [20] C.L. Chiang, M.F. Wu, D.C. Dai, Y.S. Wen, J.K. Wang, C.T. Chen, *Adv. Funct. Mater.* **2005**, *15*, 231-238.
- [21] a) Z. Xu, Z. Zhang, X. Jin, Q. Liao, H. Fu, *Chem. Asian J.* **2017**, *12*, 2985-2990; b) K. Wang, H. Zhang, S. Chen, G. Yang, J. Zhang, W. Tian, Z. Su, Y. Wang, *Adv. Mater.* **2014**, *26*, 6168-6173.

FULL PAPER

- [22] P. Gayathri, M. Pannipara, A.G. Al-Sehemi, S.P. Anthony, *New. J. Chem.* **2020**, *44*, 8680-8696.
- [23] Z. Xie, B. Yang, F. Li, G. Cheng, L. Liu, G. Yang, H. Xu, L. Ye, M. Hanif, S. Liu, D. Ma, Y. Ma, *J. Am. Chem. Soc.* **2005**, *127*, 14152-14153; b) Z. Xie, H. Wang, F. Li, W. Xie, L. Liu, B. Yang, L. Ye, Y. Ma, *Cryst. Growth Des.* **2007**, *7*, 2512-2516.
- [24] C.R. Martinez, B.L. Iverson, *Chem. Sci.* **2012**, *3*, 2191-2201.
- [25] a) J.D. Chai, M. Head-Gordon, *Phys. Chem. Chem. Phys.* **2008**, *10*, 6615-6620; b) Gaussian 09, Revision **D.01**, M.J. Frisch, W.G. Trucks, H.B. Schlegel, G.E. Scuseria, M.A. Robb, J.R. Cheeseman, G. Scalmani, V. Barone, B.G. Mennucci, A. Petersson, H. Nakatsuji, M. Caricato, X. Li, H.P. Hratchian, A.F. Izmaylov, J. Bloino, G. Zheng, J.L. Sonnenberg, M. Hada, M. Ehara, K. Toyota, R. Fukuda, J. Hasegawa, M. Ishida, T. Nakajima, Y. Honda, O. Kitao, H. Nakai, T. Vreven, J.A. Montgomery Jr., J.E. Peralta, F. Ogliaro, M. Bearpark, J.J. Heyd, E. Brothers, K.N. Kudin, V.N. Staroverov, R. Kobayashi, J. Normand, K. Raghavachari, A. Rendell, J.C. Burant, S.S. Iyengar, J. Tomasi, M. Cossi, N. Rega, J.M. Millam, M. Klene, J.E. Knox, J.B. Cross, V. Bakken, C. Adamo, J. Jaramillo, R. Gomperts, R.E. Stratmann, O. Yazyev, A.J. Austin, R. Cammi, C. Pomelli, J.W. Ochterski, R.L. Martin, K. Morokuma, V.G. Zakrzewski, G.A. Voth, P. Salvador, J.J. Dannenberg, S. Dapprich, A.D. Daniels, Ö. Farkas, J.B. Foresman, J.V. Ortiz, J. Cioslowski, D.J. Fox. C.T. Wallingford, Gaussian, Inc. 2009.
- [26] Y. Shen, Z. Zhang, H. Liu, Y. Yan, S. Zhang, B. Yang, Y. Ma, *J. Phys. Chem. C* **2019**, *123*, 13047-13056.
- [27] E.F. Valeev, V. Coropceanu, D.A. da Silva Filho, S. Salman, J.L. Brédas, *J. Am. Chem. Soc.* **2006**, *128*, 9882-9886.
- [28] P.J. Holliman, M. Mohsen, A. Connell, M.L. Davies, K. Al-Salihi, M.B. Pitak, G.J. Tizzard, S.J. Coles, R.W. Harrington, W. Clegg, C. Serpa, O.H. Fontes, C. Charbonneau, M.J. Carnie, *J. Mater. Chem.* **2012**, *22*, 13318-13327.
- [29] J. Shi, S.J. Yoon, L. Viani, S.Y. Park, B. Milián-Medina, J. Gierschner, *Adv. Opt. Mater.* **2017**, *5*, 1700340.
- [30] a) M. Johnsen, M.J. Paterson, J. Arnbjerg, O. Christiansen, C.B. Nielsen, M. Jørgensen, P.R. Ogilby, *Phys. Chem. Chem. Phys.* **2008**, *10*, 1177-1191; b) Y. Zhang, M. Yiang, G.C. Han, K. Zhao, B.Z. Tang, K.S. Wong, *J. Phys. Chem. C* **2015**, *119*, 27630-27638.
- [31] L. Kong, J.X. Yang, H.P. Zhou, S.L. Li, F.Y. Hao, Q. Zhang, Y.L. Tu, J.Y. Wu, Z.M. Xue, Y.P. Tian, *Sci. China Chem.* **2013**, *56*, 106-116.
- [32] H. Mustroph, K. Reiner, B. Senns, J. Mistol, S. Ernst, D. Keil, L. Hennig, *Chem. Eur. J.* **2012**, *18*, 8140-8149.
- [33] X. Cheng, D. Li, Z. Zhang, H. Zhang, Y. Wang, *Org. Lett.* **2014**, *16*, 880-883.
- [34] Weighted averages from triexponential (**R**) and biexponential (**IR**) fluorescence decays.

FULL PAPER

Entry for the Table of Contents



Intense near infrared shining: Push-pull substituted stilbenes, decorated with a pair of side phenyls, form solid-state emitting polymorphs. Parallel offset face-to-face packing of side phenyls enabled to form crystal consisting of the electronically coupled isolated dimers, showing rare excimer type intense emission in the near infrared region.